Nonlinear Waves.
Solitons. Autowaves. Self-Organization

Izvestiya Vysshikh Uchebnykh Zavedeniy. Applied Nonlinear Dynamics. 2023;31(2)

Article DOI: 10.18500/0869-6632-003032

Influence of parametric instability on spin pumping by dipole-exchange magnetostatic surface waves in YIG–Pt structures

M. E. Seleznev[1], *Y. V. Nikulin*[1,2], *Y. V. Khivintsev*[1,2], *S. L. Vysotskii*[1,2], *A. V. Kozhevnikov*[1], *V. K. Sakharov*[1,2], *G. M. Dudko*[1], *Y. A. Filimonov*[1,2] ✉

[1]Saratov Branch of Kotelnikov Institute of Radioengineering and Electronics of the RAS, Russia
[2]Saratov State University, Russia
E-mail: mixanich94@mail.ru, yvnikulin@gmail.com, khivintsev@gmail.com, vysotsl@gmail.com, kzhavl@gmail.com, valentin@sakharov.info, dugal_2010@hotmail.com, ✉yuri.a.filimonov@gmail.com
Received 13.12.2022, accepted 3.02.2023, available online 20.03.2023, published 31.03.2023

Abstract. The *purpose* of this work is to study the influence of four-magnon (4M) parametric instability on spin pumping by dipole-exchange magnetostatic surface waves (MSSW) with the help of the inverse spin Hall effect (ISHE) in structures based on yttrium-iron garnet (YIG) and platinum (Pt). *Methods.* The experiments were carried out using the delay line structures based on YIG(900 nm)/Pt(9 nm) where electromotive force (EMF) induced by ISHE demonstrates a growth at the frequencies of the resonant interaction between MSSW and volume exchange modes. The frequency dependencies of the amplitude and phase for the delay line structure and EMF ($U(f)$) from the platinum layer were studied as a function of the MSSW power. *Results.* It was shown that the resonant EMF growth at the frequencies of dipole-exchange resonances is caused by the presence of Van Hove singularities in the density of states for spin waves at such frequencies that leads to an increase in the efficiency of electron-magnon scattering at the YIG–Pt interface. A growth in MSSW power beyond the threshold of 4M instability development results in a "smoothing" of resonant particularities in the EMF frequency dependence $U(f)$ that can be explained by decreasing efficiency of spin pumping due to destruction of dipole-exchange resonances and related singularities in the density of states of spin waves. *Conclusion.* Obtained results may be of interest for the development of highly sensitive spin current detectors, as well as for the implementation of spintronic devices.

Keywords: parametric spin waves, spin pumping, YIG–Pt structures, electron-magnon decay, Van Hove singularities.

Acknowledgements. The work was supported by RSF grant No. 22-19-00500.

For citation: Seleznev ME, Nikulin YV, Khivintsev YV, Vysotskii SL, Kozhevnikov AV, Sakharov VK, Dudko GM, Filimonov YA. Influence of parametric instability on spin pumping by dipole-exchange magnetostatic surface waves in YIG–Pt structures. Izvestiya VUZ. Applied Nonlinear Dynamics. 2023;31(2):225–242. DOI: 10.18500/0869-6632-003032

Introduction

The generation and detection of spin currents in heterostructures based on films of uttrium garnet (YIG) and platinum (Pt) attract great attention in both fundamental and applied spintronics [1–4]. Spin currents in such heterostructures are generated using spin pumping by coherent [5–9] or incoherent (thermal) [10,11] or parametric [12–15]) spin waves (SW). The density of the spin current J_S injected into the Pt film is determined by the processes of electron-magnon scattering at the YIG/Pt boundary [16]. To detect the spin current injected into platinum, the inverse spin Hall effect (ISHE) [17,18] is used. It converts the spin current J_S into electric current

$$J_c \sim |J_S| \cdot [\vec{n} \times \vec{\sigma}], \tag{1}$$

where $\vec{n}$ and $\vec{\sigma}$ are unit vectors along the normal to the YIG/Pt interface and the magnetization $\vec{M}$ of the YIG film at the interface [1,5–15]. In experiments on spin pumping by coherent microwave spin waves, the EMF $U \sim |J_c|$ generated at the ends of the film is measured. In this case, the efficiency of spin pumping is usually characterized by the ratio S of the EMF value U to the incident microwave power ($S = U/P$) [5].

One of the parameters determining the efficiency of electron-magnon scattering at the YIG/Pt boundary is the density of states $\eta(f)$ in the spin wave spectrum of the YIG/Pt [16] structure. A special role is played by the frequencies f^* of Van Hove singularities [19] in the density of magnon states ($\eta(f^*) \to \infty$), which correspond to frequencies with small values of group velocity v_g SW ($v_g(f^*) \to 0$). Examples of such frequencies f^*, in relation to the pumping of spin current by MSSW, are the long-wave (f_0) and short-wave (f_s) boundaries in the spectrum [20–22], as well as the frequencies f_N, at which MSSW resonantly interacts with the exchange modes of the YIG film and dipole exchange waves are formed [23–25]:

$$f_N = \sqrt{(f_H + f_{ex})(f_H + f_{ex} + f_m)}, \tag{2}$$

where $f_{ex} = 2\gamma A Q^2/M$, A is the exchange stiffness in the YIG, $\gamma = 2.8$ MHz/Oe is gyromagnetic ratio in YIG, $f_H = \gamma H$, $f_m = \gamma 4\pi M$, $Q = \sqrt{k^2 + k_{\perp,N}^2}$ is total wave number of SW, k and $k_{\perp,N} = \pi N/d$ are components of the wave number Q in the plane and in thickness d of the film, N is the number of the exchange mode characterizing the number of half-waves of the exchange wave across the thickness d. The values of the volt-watt sensitivity parameter S of spin current detectors at frequencies f^* can increase by almost an order of magnitude [24,25]. This is important for the successful design of spintronics devices using microwave spin pumping. The purpose of this work is to study the influence of four-magnon (4M) parametric instability on spin pumping by dipole-exchange MSSW in the YIG/Pt structures.

4M parametric instability occurs when the power of the pump wave is above a certain threshold level $P_{\text{th}}^{\text{4M}}$ ($P > P_{\text{th}}^{\text{4M}}$) and when the conservation laws [26–28]:

$$2f_p = f_1 + f_2, \quad 2\vec{k}_p = \vec{k}_1 + \vec{k}_2, \tag{3}$$

where the frequencies $f_{p,1,2}$ and the wave vectors $\vec{k}_{p,1,2}$ correspond to the pump wave and parametric SWs (PSW). The effect of the processes (3) on spin pumping in the YIG/Pt structures was studied both under conditions of excitation by ferromagnetic resonance (FMR) [12–15,29–33] and traveling dipole magnetostatic waves (MSW) [6,22]. It has been shown that the decrease in microwave magnetic susceptibility at $P > P_{\text{th}}^{\text{4M}}$, as well as self-oscillations and bistability in the PSW system [26–28] in the YIG/Pt structures lead to a nonlinear dependence $U = U(P)$ [6,12,22,29–31], to oscillations [32] and EMF bistabilities [33].

Spin pumping by dipole-exchange MSSW with a power below the 4M instability threshold ($P < P_{\text{th}}$) was considered in [5, 24, 25]. At the same time, in the work [5], an increase in the sensitivity S of spin pumping was observed during resonant excitation of the standing mode of a rectangular YIG resonator at the frequency of hybridization between the lateral and thickness modes in the YIG film with $d \approx 2.1$ microns [12]. In the works of [24, 25], spin pumping by traveling dipole-exchange MSSW was considered in the delay line structures based on YIG/Pt structures. At the same time, in the work [25], the studies were carried out with a structure based on a two-layer exchange-coupled YIG film. In [24], a structure based on a YIG film with $d \approx 0.9$ microns was used. This paper presents the results of a study of the influence of processes (3) on the generation of spin current by traveling dipole-exchange MSSW in the YIG/Pt structure with the parameters of a YIG film identical to the work of [24].

1. The studied structures and methods of the experiment

Fig. 1 schematically shows the delay line (DL) structure for the MSSW based on the integrated YIG/Pt structures. The DL structure was made on the basis of a YIG film with a thickness $d \approx 0.9$ microns with an effective saturation magnetization $4\pi M \approx 1800$ G, an exchange stiffness $A = 4.7 \cdot 10^{-7}$ erg/cm and a relaxation parameter $\alpha \approx 3 \cdot 10^{-4}$ (FMR line width $2\Delta H \approx 0.5$ Oe) grown on a substrate of gadolinium-gallium garnet (GGG) with a crystallographic orientation (111).

Pt-film of thickness $t \approx 9$ nm and resistivity $\rho \approx 0.41 \cdot 10^{-6}$ Om·m ($R_{\square} \approx 50.1$ Om) was grown on the YIG surface by magnetron sputtering. A microstrip with length $L \approx 220$ μm and width $W \approx 200$ μm was formed from Pt film by photolithography and ion etching.

Then, by the lift-off technique, copper microantennas for SW and contacts to the Pt film were formed on the surface of the YIG, indicated by the numbers 1, 2 and 3, 4 in Fig. 1. The antennas had an aperture $w \approx 250$ microns, a width $b \approx 4$ microns, a thickness $h \approx 0.5$ microns and were located at a distance $D \approx 250$ microns from each other. The copper contacts had a width of about 15 microns and overlapped the platinum film with a width W. Also, a DL structure without a platinum film and copper contacts 3 and 4 was fabricated to define the characteristics of the MSSW in the YIG film and analyze changes in characteristics caused by Pt and contacts 3 and 4.

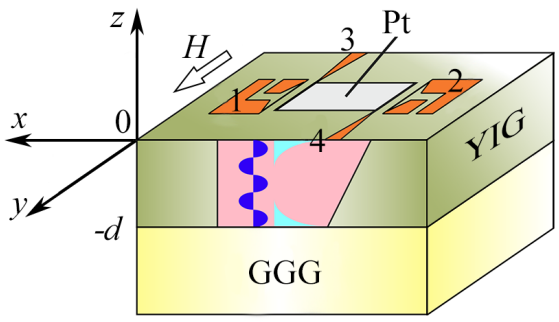

Fig. 1. The delay line on MSSW based on a YIG/Pt microstructure: 1, 2 — copper microantennas of spin waves (SW); 3, 4 — copper contacts to Pt film. Direction of magnetic field H is denoted by an arrow. In the inset, a character of magnetization $|m(z)|$ distribution across the thickness is schematically shown for dipole Damon–Eshbach MSSW, exchange volume and surface modes [23] by pink, blue and light-blue colours, respectively (color online)

The structure under study was placed between the poles of the electromagnet in a in-plane magnetic field $\vec{H}$ that was oriented along microantennas and could vary within $-2473 < H < 2473$ Oe. The used geometry corresponds to the excitation and propagation of the Damon–Eshbach MSSW [20]. To measure the transmission coefficients of the DL structure, the Keysight M9374A vector circuit analyzer was used, which was connected to microantennas 1 and 2 using Picoprobe Model 50A microwave microprobes. The frequency dependences of the coefficients of transmission $S_{12}(f)$ between antennas 1 and 2 and reflection $S_{22}(f)$ from antenna 2 were measured at various levels of incident power P_{in} and values H. The incursion of the MSSW phase $\Theta(f)$ in the structure was defined as $\Theta(f) = \text{arctg}(\,\text{Im}\,[S_{12}(f)]/\,\text{Re}\,[S_{12}(f)])$ and was used to calculate the MSSW wave number $k(f) = \Theta(f)/D$ [34].

The measurement of the EMF $U(f)$ generated at contacts (3, 4) to the Pt film during the propagation of MSSW at a frequency f was carried out using a selective voltmeter (SR830) in the mode of modulation of incident microwave power P_{in} by a meander with a frequency $\Omega_t \approx 11.33$ kHz. This approach to measure the $U(f)$ signal makes it possible to reduce the influence of noise and spurious signals on the measurement process, to reduce the contribution from the thermal EMF caused by inhomogeneous heating of the structure by microwave power. At the same time, the contribution to EMF from electron-magnon scattering processes, characterized by the times $\tau_{e-m} \sim 10^{-12}$ s [35], tracks power modulation without inertia.

To study the effect of 4M parametric processes on spin current generation, it is necessary to create conditions under which parametric processes of three-magnon (3M) decay are prohibited at the pump frequency f_p. These processes are characterized by the lowest levels of threshold power P_{th}^{3M} ($P_{\text{th}}^{3M} \ll P_{\text{th}}^{4\text{M}}$) [26–28]. This can be achieved if the following condition is met [36–38]:

$$f_p > 2(f_H + f_{ex}). \tag{4}$$

Regarding the dipole MSSW, when the contribution of the frequency f_{ex} of the exchange shift of the "bottom" of the spectrum can be neglected, the condition (4) in the YIG films is fulfilled in the entire frequency band of the MSSW at a field $H > 2\pi M \approx 875$ Oe [36–38]. Further, the results of experiments at $H = 939$ Oe will be discussed. At the same time, the achievement of the conditions for the development of 4M instability of the MSSW was determined by the standard method [22, 39, 40] tracking the magnitude decrease for the transmission coefficient $|S_{12}(f, P)|$
at $P > P_{\text{th}}^{4\text{M}}$.

2. Results and discussion

In this section, we discuss the results proving that the studied YIG/Pt structures support the propagation of dipole-exchange MSSW. At the frequencies of dipole exchange resonances, a resonant increase in the efficiency of spin pumping is observed, associated with van Hove singularities. In order to discuss in more detail the effect of 4M parametric processes on spin pumping by dipole-exchange MSSW in YIG/Pt structures, nonlinear dipole-exchange MSSWs in the DL structure based on a YIG film without Pt are preliminarily considered.

2.1. Nonlinear dipole-exchange MSSW in a YIG film. Fig. 2, *a* shows the transmission spectra of the DL structure based on the YIG film measured at various levels of incident power P_{in}. It can be seen that at the power level $P_{\text{in}} = -20$ dBm, resonant "dips" are observed at frequencies marked with asterisks in the dependencies $|S_{12}(f, P)|$. This is typical for the resonant interaction [23, 41] of dipole MSSW with exchange volume modes of the film at frequencies f_N, which can be calculated according to the formula (2).

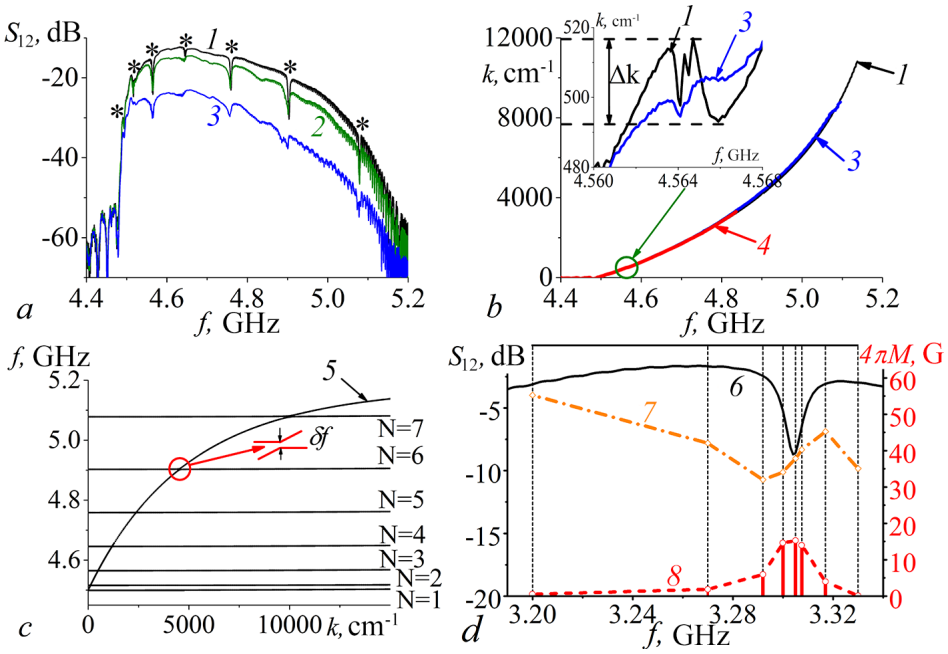

Fig. 2. Measurements results of frequency dependencies of transmission coefficient $S_{12}(f)$ (a) and dispersions $k(f)$ (b) in the structures based on YIG films at $H = 939$ Oe and $P_{\text{in}} = -20$ (*1*), -10 (*2*), 0 (*3*) dBm; curve *4* shows the measured dispersion in the YIG/Pt structure at $P_{\text{in}} = -20$ dBm; the inset to Fig. b shows the part of dispersion with anomalous behavior; c — calculated spectrum of dipole-exchange MSSW in the YIG film with the numbers of exchange modes $N = 1...7$ where the curve *5* shows the dispersion of Damon–Eshbach MSSW; the inset to Fig. c demonstrates the character of dispersion repulsion in the vicinity of the resonance of MSSW with the exchange mode with number $N = 6$ and formation of a spectrum "gap" $\delta f \approx 5$ MHz; d — micromagnetic modeling of the frequency dependencies in the vicinity of the dipole-exchange resonance with the number $N = 5$: the curve *6* corresponds to $S_{12}(f)$, the curves *7* and *8* correspond to the amplitude of magnetization $|m(z)|$ at the border $z = 0$ and to the amplitude of volume exchange mode, respectively. The character of volume mode distribution is shown by blue color in the inset to Fig. 1 (color online)

The resonant increase in losses at frequencies f_N is accompanied, in accordance with the Kramers–Kronig ratio, by the formation of anomalous regions in the law of dispersion $k(f)$ for MSSW [41, 42]. This can be seen from the inset to Fig. 2, b, which presents the measurement results for $k(f)$ in a YIG film at the frequency of the resonance between MSSW and exchange mode with the number $N = 3$. The measured dispersion outside the frequencies of dipole exchange resonances is shown in Fig. 2, b curve *1*. In general, it corresponds to Damon–Eshbach [20] law of dispersion:

$$f^2 = f_0^2 + 1/4 f_m^2 (1 - \exp(-2kd)). \tag{5}$$

where $f_0^2 = f_H^2 + f_H \cdot f_m$.

In Fig. 2, c the calculated spectrum $f = f(k)$ of the dipole exchange MSSW in a film with selected parameters are shown. The calculation was performed in a non-dissipative approximation within the framework of the [23] approach. In the inset to Fig. 2, c the character of the dispersion in the vicinity of the MSSW resonance with the exchange mode having number $N = 6$ is given. It can be seen that the dispersion curves repulse each other and form a "gap" $\delta f \approx 5$ MHz in the spectrum. With a sufficiently large dissipation [41, 42], the "gap" in the spectrum disappears. But there is an abnormal area in dispersion (inset to Fig. 2, b) and a resonant increase in losses (see narrow "dips" in $|S_{12}(f, P)|$ dependence in Fig. 2, a). It should be noted that at frequencies f_N, dispersion regions $f = f(k)$ with a low group velocity $v_g(f_N) = 2\pi \partial f / \partial k \to 0$ are formed

in the spectrum. One should expect that Van Hove singularities $\eta(f_N) \to \infty$ [19] will occur at frequencies f_N in the density of states for SW.

Fig. 2, *d* presents the results of micromagnetic modeling (performed according to the approach [43–45] for the frequency dependence of the wave transmission coefficient (curve *6*) as well as magnetization magnitudes at YIG film surface $|m(z = 0)|$ (curve *7*) and magnitude of volume exchange wave (curve *8*) in the vicinity of the frequency of the dipole-exchange resonance with $N = 5$. The character of the amplitude distribution of the volume mode $|m(z)|$ over the film thickness is illustrated by the oscillating blue inset to Fig. 1. At the frequency of the dipole exchange resonance, a resonant increase in losses occurs (curve *6*). It is accompanied by the fact that the magnetization amplitude at the boundary $z = 0$, to which the Damon–Eschbach MSSW is "pressed", decreases (curve *7*). At the same time, the amplitude of the volume exchange mode increases (curve *8*). This behavior of magnetization reflects the redistribution of energy between two oscillatory subsystems under resonance conditions.

When the power of the MSSW is above the threshold of parametric instability $P > P_{\text{th}}^{\text{4M}}$, the amplitude of the coefficient S_{12} decreases due to the influence of nonlinear attenuation and a drop in high-frequency magnetic susceptibility. This can be seen from the comparison of the curves *1*, *2* and *3* in Fig. 2, *a*. With the growth of P, the resonant features in the dependence $|S_{12}(f, P)|$ are smoothed out. At the same time, the "amplitude" Δk of the anomalous region in the law of dispersion at frequencies f_N decreases (Fig. 2, *b*). In general, this behavior of the dependencies $|S_{12}(f, P)|$ and $k(f)$ with an increase in P_{in} indicates the destruction of dipole exchange resonances by processes (3). For the DL structure based on a YIG film, the value of $P_{\text{th}}^{\text{4M}}$ is $P_{\text{th}}^{\text{4M}} \approx 20$ μW. The specified threshold power values can be related with the threshold values of the magnetization amplitude $m_{\text{th}}^{\text{4M}}$ MSSW using the ratio [39, 40]:

$$m_{\text{th}}^{\text{4M}} = \sqrt{\frac{P_{\text{th}}}{v_{\text{g}} \cdot w \cdot d}}, \tag{6}$$

where the product $w \cdot d$ determines the cross-sectional area of the film through which the power of the MSSW is transferred. Values of m_{th} calculated using (6) for parameters corresponding to Fig. 1, are in the case of 4M processes $m_{\text{th}}^{\text{4M}} \approx 1.2$ G. This is consistent with an estimate within the framework of Suhl's theory for homogeneous pumping [26–28] $m_{\text{th}}^{\text{4M}} \approx \sqrt{M \cdot \Delta H/(4\pi)} \approx 1.7$ G.

2.2. The effect of 4M parametric processes on spin pumping by dipole-exchange MSSW in the YIG/Pt structure. Before discussing the influence of processes (3) on the generation of EMF in the YIG/Pt structure due to spin pumping by dipole-exchange MSSW, let us consider some changes in the characteristics of the MSSW propagation caused by metallization of the YIG film. Firstly, the deposition of Pt film and contacts 3, 4 between the input and output transducers (Fig. 1) leads to a noticeable reduction of the MSSW compared to the case of the DL structure based on the YIG film (curves *1* and *2* in Fig. 3, *a*). We found out that the mentioned increase in MSSW losses is mostly due to copper contact microstrips to platinum. This was proven with the help of the DL structure without a Pt film, but with copper contacts 3 and 4, and obtaining for it the dependence $S_{12}(f)$, which differs from the curve *1* in Fig. 3, *a* within 1-2 dB. It should be noted that the effect of conduction electrons on the dispersion and attenuation of MSSW is characterized by the spin-electron coupling parameter $G = h/(k \cdot l_{\text{sk}}^2)$ [46]. With a metal thickness $h = 500$ nm, a skin layer depth $l_{\text{sk}} \approx 1$ μm and a wave number range $1500 < k < 8000$ sm^{-1} the parameter G takes the values $3 > G > 0.6$. At such values of G, there are no propagating MSSW in the metallized YIG film [47, 48].

However, the results of measurement of the dependence $k = k(f)$ for the YIG/Pt structure turned out to be close to the case of a non-metallized film (curve *4*, Fig. 2, *b*). This can be

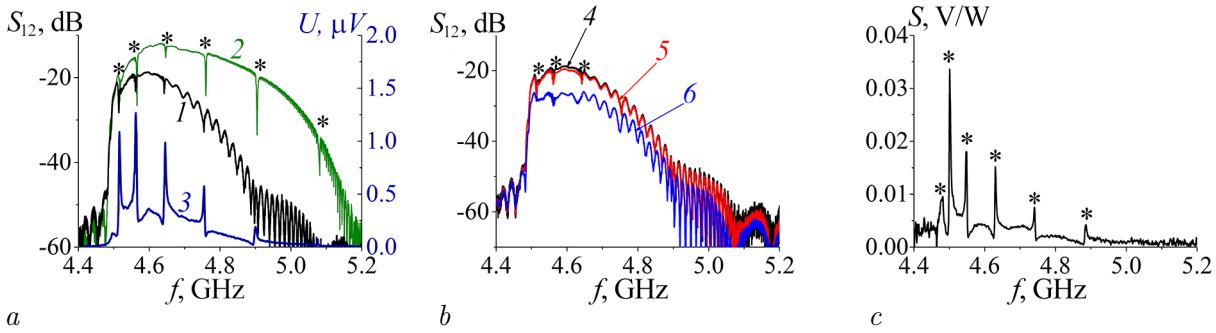

Fig. 3. YIG/Pt structure. *a* — Frequency dependencies $S_{12}(f)$ and $U(f)$ (curves *1* and *3*) at $P_{\text{in}} = -10$ dBm; the curve *2* shows the $S_{12}(f)$ dependence in the delay line structure based on YIG film; *b* — $S_{12}(f)$ at $P_{\text{in}} = -20$ (*4*), -10 (*5*) and 0 (*6*) dBm; *c* — The frequency dependence of volt-watt sensitivity $S(f)$ at $P_{\text{in}} = -10$ dBm (color online)

explained as follows. The width of the copper contact of the order of 15 microns fits no more than four wavelengths of MSSW. The length of the film area under the copper contacts in the direction of MSSW propagation is approximately 12% of the distance between the input and output antennas. For the part of the DL structure that is covered with a Pt film at $t \approx 9$ nm and $l_{\text{sk}} \approx 7$ μm, parameter $G < 0.1$ and the effect of platinum on the dispersion of MSSW is extremely small [22].

Secondly, the introduced electronic losses lead to a noticeable increase in the level of input power P_{in}, which is necessary to reach the 4M threshold of parametric instability of the MSSW. Let's compare the transmission spectra of $|S_{12}(f, P)|$ at $P_{\text{in}} = -20$ dBm and $P_{\text{in}} = -10$ dBm, which are shown by the curves *1* and *2* in Fig. 2, *a* and fig. 3, *b*. We see that in the YIG/Pt structure, changes caused by the development of parametric instability at $P_{\text{in}} = -10$ dBm are observed only in a narrow frequency range. While in the YIG film without platinum, they are visible much more in the entire frequency band.

With this in mind, let us now turn to the results of measurements of the effect of EMF generation in the YIG/Pt structure depending on the power level P. In Fig. 3, *a* the curve *3* shows the frequency dependence of the EMF $U(f)$ at the level of incident power $P_{\text{in}} = -20$ dBm. One can see that at the frequencies marked with «*», the EMF increases resonantly. At the same time, the volt-watt sensitivity S also demonstrates an increase in values by almost an order of magnitude (Fig. 3, *c*). We associate this increase in EMF with the occurrence of van Hove singularities in the density of states $\eta(f)$ at frequencies f_N. This should lead to an increase in the efficiency of electron-magnon scattering [16].

Indeed, if we try to explain the EMF growth by the proportionality of the spin current density $|J_s|$ to the magnetization amplitude at the interface $|m(z = 0)|$, then according to the results of micromagnetic modeling (curve *6* in Fig. 2, *d*) the EMF value should decrease in proportion to the decrease in $|m(z = 0)|$ at the resonance frequency f_N. Besides, from the comparison of the values of EMF or sensitivity S for resonances with different numbers N (Fig. 3, *c*), it follows that these values are not directly related to the values of the projection of the wavenumber on the normal to the film $k_{\perp,N} = \pi N/d$.

Let us now consider the influence of 4M parametric processes on the generation of EMF by dipole-exchange MSSW. In Fig. 4, *a* the results of measurement of $U(f)$ dependencies at various levels of incident power are given. The EMF at resonant frequencies f_N decreases with an increase in P_{in}. With a further increase in P_{in}, the resonant features in the dependence $U(f)$ may disappear. This is illustrated in Fig. 4, *b*, where the dependencies $U = U(P_{\text{in}})$ are given for the frequency $f_1 \approx 4.952$ GHz, located between the resonant frequencies $f_{N=3}$ and $f_{N=4}$, and

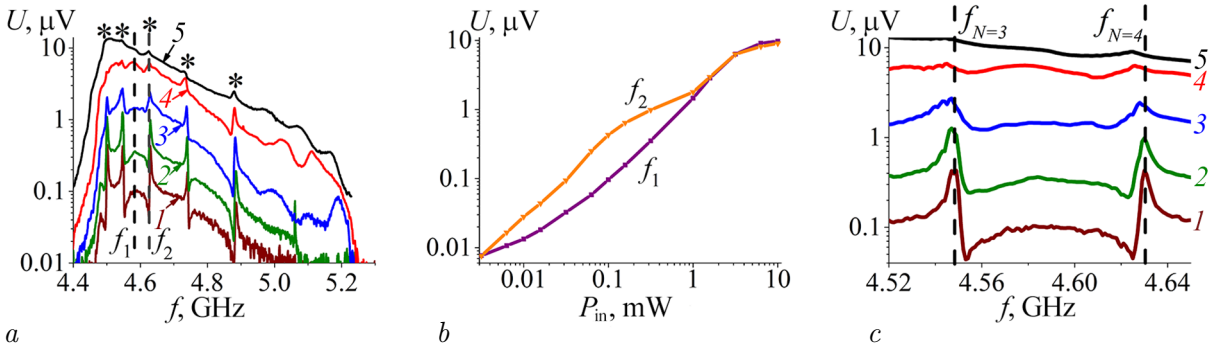

Fig. 4. *a* — The curves 1–5 show the $U(f)$ dependencies at $P_{\text{in}} = -10$; -5; 0; 5; 10 dBm; *b* — the dependencies $U = U(P_{\text{in}})$ at frequencies $f_1 \approx 4.582$ GHz and $f_2 \approx 4.631$ GHz, which position is shown by vertical dash lines in Fig. *a*; *c* — the influence of MSSW power on position of dipole-exchange resonances with the numbers $N = 3$ and $N = 4$; vertical dash lines show the EMF peak position at frequencies $f_{N=3}$ and $f_{N=4}$ at $P_{\text{in}} = -10$ dBm (color online)

$f_2 \approx 4.631$ GHz, which at $P_{\text{in}} = -10$ dBm corresponds to the resonant frequency $f_{N=4}$. It can be seen that the dependencies $U = U(f_{1,2}, P_{\text{in}})$ are nonlinear and tend to saturate with the growth of P_{in}. At the same time, the dependence $U(P_{\text{in}})$ for the frequency f_1 grows faster with the input power of $0.2 < P_{\text{in}} < 1$ mW.

This behavior can be explained by the relationship between the magnitude of the EMF peak and the amplitude Δk of the anomalous dispersion region at the frequency of the dipole exchange resonance (inset to Fig. 2, *b*). The disappearance of abnormal regions in the MSSW spectrum reflects the shutdown of the process of population of spectral regions by propagating dipole-exchange MSSW and, as a consequence, a decrease in the efficiency of electron-magnon scattering at the interface. This does not mean that the number of magnons on the interface is decreasing. On the contrary, the destruction of the dipole exchange resonance at the pumping frequency leads to a decrease in the number of magnons "moving away" from the surface into the volume of the film. The reason for the decrease in the efficiency of electron-magnon scattering is a decrease in the number of states into which a fermi particle (electron) can scatter due to the disappearance of singularities in the spin wave spectrum.

In some cases, processes (3) can contribute conversely and cause a faster growth of dependence $U(P_{\text{in}})$. This is illustrated by the dependence $U = U(f_1, P_{\text{in}})$ in Fig. 4, *b* at $0.2 < P_{\text{in}} < 1$ mW. Such behavior of $U = U(f_1, P_{\text{in}})$ is explained by the fact that parametric SW generated as a result of processes (3) populate regions of the SW spectrum with singularities in the density of states. It is important to note that, at the frequencies of van Hove singularities, the effective mass of magnons $m^{\text{def}} \sim \hbar \frac{\partial^2 f}{\partial k^2}$. It may be greater than the mass of electrons in platinum. It is intuitively clear that "heavy" magnons scatter electrons more efficiently.

We should note that the distruction of dipole-exchange resonances is caused not only by the growth of nonlinear losses resulted from the processes (3). Nonlinearity and dissipation lead to the fact that the YIG film becomes inhomogeneous in the direction of wave propagation [22, 39, 40, 49]. The dependences $\Delta k(f, P_{\text{in}})$ measured in the experiment reflect the integral phase incursion of the nonlinear wave in the DL structure [40]. At the same time, local changes in the dispersion characteristics may be much larger in magnitude.

It is also necessary to take into account the nonlinear shift of the spin wave spectrum caused by a decrease in the projection of the magnetization of the film $4\pi M_y(x)$ to the direction of the magnetic field $\vec{H}$ due to the heating of the film with microwave power and the effect of dynamic demagnetization [22, 49]:

$$4\pi M_y(x) = 4\pi M_0 \cdot (1 - \frac{m(x)^2}{M_0^2}), \tag{7}$$

where the amplitude $m(x = 0)$ is related to P_{in} through the ratio (6), and the dependence on the coordinate x reflects the attenuation of the amplitude of the MSSW $m(x)$ during propagation (Fig. 1). At the same time, all characteristic frequencies that determine the frequencies of dipole exchange resonances depend on P_{in} and the x-coordinate:

$$f_0(x) = \sqrt{f_H^2 + f_H \cdot f_m(x)}, \quad f_m(x) = \gamma 4\pi M_y(x), \tag{8}$$

$$f_N(x) = \sqrt{(f_H + f_{ex}(x))(f_H + f_{ex}(x) + f_m(x))}. \tag{9}$$

Fig. 4, *c* shows the dependences on P_{in} of the position of the maxima in the frequency dependence of the EMF for dipole exchange resonances at frequencies $f_{N=3}$ and $f_{N=4}$. We see that with increasing power and simultaneously with the "destruction" of the resonant peaks, their shift "down" in frequency occurs.

Conclusion

Thus, the influence of the processes of four-magnon parametric instability on the generation of spin current during spin pumping by dipole-exchange surface magnetostatic waves propagating in a delay line structure based on a YIG(900 nm)/Pt(9 nm) film. We have shown that the pumping efficiency increases resonantly at the frequencies of dipole exchange resonances using the detection of spin current via the EMF generated by the inverse spin Hall effect. This increase is explained by an increase in the efficiency of electron-magnon scattering due to van Hove singularities in the density of spin wave states and a large effective mass of magnons at the frequencies of dipole exchange resonances. We found that an increase in the power of surface magnetostatic waves beyond the threshold P_{th}^{4m} of the development of 4M instability leads to a "smoothing" of resonant features in the frequency dependence of EMF $U(f)$. Such an influence of 4M processes on the dependence $U(f)$ is explained by a decrease in the efficiency of spin pumping due to the destruction of dipole exchange resonances and associated singularities in the density of spin wave states in the spectrum of the YIG/Pt structure at $P > P_{\text{th}}^{4\text{M}}$. The obtained results may be of interest for the development of highly sensitive spin current detectors and spintronics devices.

References

1. Kajiwara Y, Harii K, Takahashi S, Ohe J, Uchida K, Mizuguchi M, Umezawa H, Kawai H, Ando K, Takanashi K, Maekawa S, Saitoh E. Transmission of electrical signals by spin-wave interconversion in a magnetic insulator. Nature. 2010;464(7286):262–266. DOI: 10.1038/nature08876.
2. Sinova J, Valenzuela SO, Wunderlich J, Back CH, Jungwirth T. Spin Hall effects. Rev. Mod. Phys. 2015;87(4):1213–1260. DOI: 10.1103/RevModPhys.87.1213.
3. Althammer M. Pure spin currents in magnetically ordered insulator/normal metal heterostructures. J. Phys. D: Appl. Phys. 2018;51(31):313001. DOI: 10.1088/1361-6463/aaca89.
4. Brataas A, van Wees B, Klein O, de Loubens G, Viret M. Spin insulatronics. Physics Reports. 2020;885:1–27. DOI: 10.1016/j.physrep.2020.08.006.
5. Sandweg CW, Kajiwara Y, Ando K, Saitoh E, Hillebrands B. Enhancement of the spin pumping efficiency by spin wave mode selection. Appl. Phys. Lett. 2010;97(25):252504. DOI: 10.1063/1.3528207.
6. Chumak AV, Serga AA, Jungfleisch MB, Neb R, Bozhko DA, Tiberkevich VS, Hillebrands B. Direct detection of magnon spin transport by the inverse spin Hall effect. Appl. Phys. Lett. 2012;100(8):082405. DOI: 10.1063/1.3689787.

7. Balinsky M, Ranjbar M, Haidar M, Dürrenfeld P, Khartsev S, Slavin A, Åkerman J, Dumas RK. Spin pumping and the inverse spin-hall effect via magnetostatic surface spin-wave modes in Yttrium-Iron garnet/platinum bilayers. IEEE Magn. Lett. 2015;6:3000604. DOI: 10.1109/LMAG.2015.2471276.
8. Iguchi R, Ando K, Qiu Z, An T, Saitoh E, Sato T. Spin pumping by nonreciprocal spin waves under local excitation. Appl. Phys. Lett. 2013;102(2):022406. DOI: 10.1063/1.4775685.
9. d'Allivy Kelly O, Anane A, Bernard R, Ben Youssef J, Hahn C, Molpeceres AH, Carrétéro C, Jacquet E, Deranlot C, Bortolotti P, Lebourgeois R, Mage JC, de Loubens G, Klein O, Cros V, Fert A. Inverse spin Hall effect in nanometer-thick yttrium iron garnet/Pt system. Appl. Phys. Lett. 2013;103(8):082408. DOI: 10.1063/1.4819157.
10. Uchida K, Xiao J, Adachi H, Ohe J, Takahashi S, Ieda J, Ota T, Kajiwara Y, Umezawa H, Kawai H, Bauer GEW, Maekawa S, Saitoh E. Spin Seebeck insulator. Nature Materials. 2010;9(11):894–897. DOI: 10.1038/nmat2856.
11. Agrawal M, Vasyuchka VI, Serga AA, Kirihara A, Pirro P, Langner T, Jungfleisch MB, Chumak AV, Papaioannou ET, Hillebrands B. Role of bulk-magnon transport in the temporal evolution of the longitudinal spin-Seebeck effect. Phys. Rev. B. 2014;89(22):224414. DOI: 10.1103/PhysRevB.89.224414.
12. Sandweg CW, Kajiwara Y, Chumak AV, Serga AA, Vasyuchka VI, Jungfleisch MB, Saitoh E, Hillebrands B. Spin pumping by parametrically excited exchange magnons. Phys. Rev. Lett. 2011;106(21):216601. DOI: 10.1103/PhysRevLett.106.216601.
13. Kurebayashi H, Dzyapko O, Demidov VE, Fang D, Ferguson AJ Demokritov SO. Controlled enhancement of spin-current emission by three-magnon splitting. Nature Materials. 2011; 10(9):660–664. DOI: 10.1038/nmat3053.
14. Kurebayashi H, Dzyapko O, Demidov VE, Fang D, Ferguson AJ, Demokritov SO. Spin pumping by parametrically excited short-wavelength spin waves. Appl. Phys. Lett. 2011; 99(16):162502. DOI: 10.1063/1.3652911.
15. Manuilov SA, Du CH, Adur R, Wang HL, Bhallamudi VP, Yang FY, Hammel PC. Spin pumping from spinwaves in thin film YIG. Appl. Phys. Lett. 2015;107(4):042405. DOI: 10.1063/1.4927451.
16. Tveten EG, Brataas A, Tserkovnyak Y. Electron-magnon scattering in magnetic heterostructures far out of equilibrium. Phys. Rev. B. 2015;92(18):180412. DOI: 10.1103/PhysRevB.92.180412.
17. Saitoh E, Ueda M, Miyajima H, Tatara G. Conversion of spin current into charge current at room temperature: Inverse spin-Hall effect. Appl. Phys. Lett. 2006;88(18):182509. DOI: 10.1063/1.2199473.
18. Maekawa S, Adachi H, Uchida K, Ieda J, Saitoh E. Spin current: Experimental and theoretical aspects. J. Phys. Soc. Jpn. 2013;82(10):102002. DOI: 10.7566/JPSJ.82.102002.
19. Van Hove L. The occurrence of singularities in the elastic frequency distribution of a crystal. Phys. Rev. 1953;89(6):1189–1193. DOI: 10.1103/PhysRev.89.1189.
20. Damon RW, Eshbach JR. Magnetostatic modes of a ferromagnet slab. Journal of Physics and Chemistry of Solids. 1961;19(3–4):308–320. DOI: 10.1016/0022-3697(61)90041-5.
21. Nikulin YV, Seleznev ME, Khivintsev YV, Sakharov VK, Pavlov ES, Vysotskii SL, Kozhevnikov AV, Filimonov YA. EMF generation by propagating magnetostatic surface waves in integrated thin-film Pt/YIG structure. Semiconductors. 2020;54(12):1721–1724. DOI: 10.1134/S106378262012026X.
22. Seleznev ME, Nikulin YV, Khivintsev YV, Vysotskii SL, Kozhevnikov AV, Sakharov VK, Dudko GM, Pavlov ES, Filimonov YA. Influence of three-magnon decays on electromotive force generation by magnetostatic surface waves in integral YIG – Pt structures. Izvestiya VUZ. Applied Nonlinear Dynamics. 2022;30(5):617–643. DOI: 10.18500/0869-6632-003008.

23. De Wames RE, Wolfram T. Dipole-exchange spin waves in ferromagnetic films. J. Appl. Phys. 1970;41(3):987–993. DOI: 10.1063/1.1659049.
24. Seleznev ME, Nikulin UV, Sakharov VK, Khivintsev UV, Kozhevnikov AV, Vysotskii SL, Filimonov UA. Influence of the resonant interaction of surface magnetostatic waves with exchange modes on the EMF generation in YIG/Pt structures. Tech. Phys. 2021;91(10): 1504–1508 (in Russian). DOI: 10.21883/JTF.2021.10.51363.136-21.
25. Nikulin YV, Kozhevnikov AV, Vysotskii SL, Seleznev ME, Khivintsev YV, Filimonov YA. Investigation of the interference of magnetostatic surface waves using the inverse spin Hall effect. Physics of the Solid State. 2022;64(9):1284–1288. DOI: 10.21883/PSS.2022.09.54167.21HH.
26. Gurevich AG, Melkov GA. Magnetization Oscillations and Waves. Boca Raton: CRC Press; 1996. 464 p.
27. Vashkovskii AV, Stalmakhov VS, Sharaevskii YP. Magnetostatic Waves in High-Frequency Electronics. Saratov: Saratov University Publishing; 1993. 312 p. (in Russian).
28. Lvov VS. Nonlinear Spin Waves. Moscow: Nauka; 1987. 272 p. (in Russian).
29. Castel V, Vlietstra N, Ben Youssef J, Van Wees BJ. Platinum thickness dependence of the inverse spin-Hall voltage from spin pumping in a hybrid yttrium iron garnet/platinum system. Appl. Phys. Lett. 2012;101(13):132414. DOI: 10.1063/1.4754837.
30. Castel V, Vlietstra N, Van Wees BJ, Ben Youssef J. Frequency and power dependence of spin-current emission by spin pumping in a thin-film YIG/Pt system. Phys. Rev. B. 2012;86(13):134419. DOI: 10.1103/PhysRevB.86.134419.
31. Jungfleisch MB, Chumak AV, Kehlberger A, Lauer V, Kim DH, Onbasli MC, Ross CA, Kläui M, Hillebrands B. Thickness and power dependence of the spin-pumping effect in Y3Fe5O12/Pt heterostructures measured by the inverse spin Hall effect. Phys. Rev. B. 2015;91(13):134407. DOI: 10.1103/PhysRevB.91.134407.
32. Watanabe S, Hirobe D, Shiomi Y, Iguchi R, Daimon S, Kameda M, Takahashi S, Saitoh E. Generation of megahertz-band spin currents using nonlinear spin pumping. Scientific Reports. 2017;7(1):4576. DOI: 10.1038/s41598-017-04901-4.
33. Ando K, Saitoh E. Spin pumping driven by bistable exchange spin waves. Phys. Rev. Lett. 2012;109(2):026602. DOI: 10.1103/PhysRevLett.109.026602.
34. Khivintsev YV, Filimonov YA, Nikitov SA. Spin wave excitation in yttrium iron garnet films with micron-sized antennas. Appl. Phys. Lett. 2015;106(5):052407. DOI: 10.1063/1.4907626.
35. Nur Kholid F, Hamara D, Terschanski M, Mertens F, Bossini D, Cinchetti M, McKenzie-Sell L, Patchett J, Petit D, Cowburn R, Robinson J, Barker J, Ciccarelli C. Temperature dependence of the picosecond spin Seebeck effect. Appl. Phys. Lett. 2021;119(3):032401. DOI: 10.1063/5.0050205.
36. Mednikov AM. Nonlinear effects under the propagation of surface spin waves in YIG films. Soviet Physics, Solid State. 1981;23(1):242–245 (in Russian).
37. Temiryazev AG. The mechanism of transformation of magnetostatic surface waves in the conditions of three-magnon decay. Soviet Physics, Solid State. 1987;29(2):313–319 (in Russian).
38. Polzikova NI, Raevskii AO, Temiryazev AG. Influence of exchange interaction on boundary of three-magnon decay of Damon-Eshbach wave in YIG thin films. Soviet Physics, Solid State. 1984;26(11):3506–3508 (in Russian).
39. Kazakov GT, Kozhevnikov AV, Filimonov YA. Four-magnon decay of magnetostatic surface waves in yttrium iron garnet films. Physics of the Solid State. 1997;39(2):288–295. DOI: https://doi.org/10.1134/1.1129801.
40. Kazakov GT, Kozhevnikov AV, Filimonov YA. The effect of parametrically excited spin

waves on the dispersion and damping of magnetostatic surface waves in ferrite films. J. Exp. Theor. Phys. 1999;88(1):174–181. DOI: 10.1134/1.558780.
41. Gulyaev YV, Bugaev AS, Zil'berman PE, Ignat'ev IA, Konovalov AG, Lugovskoi AV, Mednikov AM, Nam BP, Nikolaev EI. Giant oscillations in the transmission of quasi-surface spin waves through a thin yttrium-iron garnet (YIG) film. JETP Lett. 1979;30(9):565–568.
42. Gulyaev YV, Zil'berman PE, Lugovskoi AV. Influence of nonuniform exchange and dissipation on propagation of surface Damon-Eshback waves in ferromagnetic plate. Soviet Physics, Solid State. 1981;23(4):1136–1142 (in Russian).
43. Donahue MJ, Porter DG. OOMMF User's Guide. Interagency Report NISTIR 6376. Gaithersburg, MD: National Institute of Standards and Technology; 1999. 94 p. DOI: 10.6028/NIST.IR.6376.
44. Dvornik M, Au Y, Kruglyak VV. Micromagnetic Simulations in Magnonics. In: Demokritov S, Slavin A, editors. Magnonics. Vol. 125 of Topics in Applied Physics. Berlin: Springer; 2013. P. 101–115. DOI: 10.1007/978-3-642-30247-3_8.
45. Sakharov VK, Khivintsev YV, Dudko GM, Dzhumaliev AS, Vysotskii SL, Stognij AI, Filimonov YA. Particularities of spin wave propagation in magnonic crystals with nonuniform magnetization distribution across the thickness. Physics of the Solid State. 2022;64(9):1247–1254.
DOI: 10.21883/PSS.2022.09.54160.11HH.
46. Bugaev AS, Galkin OL, Gulyaev YV, Zilberman PE. Electrons' drag by magnetostatic wave in a layered ferrite-metal structure. Sov. Tech. Phys. Lett. 1982;8(8):485–488 (in Russian).
47. Veselov AG, Vysotsky SL, Kazakov GT, Sukharev AG, Filimonov YA. Magnetostatic surface waves in metallized YIG films. J. Commun. Technol. Electron. 1994;39(12):2067–2074 (in Russian).
48. Filimonov YA, Khivintsev YV. Interaction of magnetostatic surface and elastic volume waves in a metallized structure ferromagnet-dielectric. J. Commun. Technol. Electron. 2002;47(8):1002–1007 (in Russian).
49. Sakharov VK, Khivintsev YV, Vysotskii SL, Stognij AI, Dudko GM, Filimonov YA. Influence of input signal power on magnetostatic surface waves propagation in yttrium-iron garnet films on silicon substrates. Izvestiya VUZ. Applied Nonlinear Dynamics. 2017;25(1):35–51. DOI: 10.18500/0869-6632-2017-25-1-35-51.